Lattice screening of the polar catastrophe and hidden in-plane polarization in KNbO$_3$/BaTiO$_3$ interfaces

Pablo García-Fernández, Pablo Aguado-Puente, and Javier Junquera

Departamento de Ciencias de la Tierra y Física de la Materia Condensada, Universidad de Cantabria, Cantabria Campus Internacional,
Avenida de los Castros s/n, 39005 Santander, Spain

We have carried out first-principles simulations, based on density functional theory, to obtain the atomic and electronic structure of (001) BaTiO$_3$/KNbO$_3$ interfaces in an isolated slab geometry. We tried different types of structures including symmetric and asymmetric configurations and variations in the thickness of the constituent materials. The spontaneous polarization of the layer-by-layer non-neutral material (KNbO$_3$) in these interfaces cancels out almost exactly the "built-in" polarization responsible for the electronic reconstruction. As a consequence, the so-called polar catastrophe is quenched and all the simulated interfaces are insulating. A model, based on the modern theory of polarization and basic electrostatics, allows an estimation of the critical thickness for the formation of the two-dimensional electron gas between 33 and 36 KNbO$_3$ unit cells. We also demonstrate the presence of an unexpected in-plane polarization in BaTiO$_3$ localized at the p-type TiO$_2$/KO interface, even under in-plane compressive strains. We expect this in-plane polarization to remain hidden due to angular averaging during quantum fluctuations unless the symmetry is broken with small electric fields.

I. INTRODUCTION

The surprising discovery by Ohtomo and Hwang[1] of a metallic state at the interface between two good band insulating oxides, LaAlO$_3$ and SrTiO$_3$, has triggered a large amount of new studies on polar oxide interfaces.[2] Indeed, the quasi-two-dimensional electron gas (2DEG) that forms when LaAlO$_3$ is grown on top of a TiO$_2$ terminated (001)-surface of SrTiO$_3$, i.e., when the interface between the two materials is LaO/TiO$_2$, displays very different properties from those generated at interfaces between standard III-V semiconductors (such as GaAs and Al$_x$Ga$_{1-x}$As). Among them we find conducting carrier densities and electron effective masses orders of magnitude larger than those found at semiconductor interfaces.[3] It is also fascinating how, depending on growth conditions, magnetic[4] and superconducting[5] ground states have been experimentally identified at this interface between nonmagnetic insulating oxides. Very recently, two independent groups have proven how both magnetic and superconducting states might even coexist on the same sample,[6,7] a very unexpected result since magnetic order is usually considered detrimental to superconductivity. As a consequence of all these phenomena, interfaces in polar oxides can open the door to novel implementations of field effect transistors and to a new era of oxide electronics.[3,8]

Despite this recent activity, many fundamental questions regarding the origin and confinement of the 2DEG remain highly debated. Different models have been proposed to explain the experimental results. The pioneering one invokes the so-called "polar catastrophe"[9] that arises from the polarization discontinuity[10] between the III-III polar LaAlO$_3$ film and the II-IV nonpolar SrTiO$_3$ layers along the [001] direction. Indeed, from the formal ionic charge point of view, LaAlO$_3$ can be described as a succession of positive (La^{+3}O^{-2})$^{+1}$ and negative (Al^{+3}O$_2^{-2}$)$^{-1}$ layers, while the alternating (Sr^{+2}O^{-2})^0 and (Ti^{+4}O$_2^{-2}$)^0 layers of the perovskite structure of SrTiO$_3$ are charge neutral. But, aside this first rationalization, other explanations can be found in the literature for the origin of the 2DEG, among them (i) the interlayer mixing between LaAlO$_3$ and SrTiO$_3$ and nonabruptness of the interfaces (with the formation of a few monolayers of metallic La$_{1-x}$Sr$_x$TiO$_3$[11]), (ii) doping due to oxygen vacancies[12,13] (including those produced in surface redox reactions[14]), and/or (iii) the presence of charged defects and adsorbates.[15,16] All these models highlight the importance of the growth conditions of these structures for the appearance and the behavior of the functional properties of the 2DEG.

One of these properties, that is well reproduced by different experimental groups on many samples grown with a variety of techniques, is the existence of a critical thickness, t_c, in the number of layers of LaAlO$_3$ for the formation of the 2DEG. Thiel and coworkers[17] have demonstrated that, for the interfaces to be conducting, the number of layers of LaAlO$_3$ has to be larger than four unit cells. The thickness of the polar layer increases up to five unit cells in n-type LaVO$_3$/SrTiO$_3$ interfaces.[18] These observations are consistent with the fact that the conductivity of SrTiO$_3$-LaAlO$_3$-SrTiO$_3$ heterostructures with dissimilar interfaces is reduced if their p-type (AlO$_2$/SrO) and n-type (LaO/TiO$_2$) interfaces are spaced by less than six unit cells.[19,20] Remarkably, even below the critical thickness, a metal-insulator transition can be driven by an external electric field.[15,17] These studies suggested the possibility of the design of new polar interfaces where the appearance of the 2DEG could be switched on and off by the action of an external perturbation.

Along this line, the replacement of one (or the two) materials at the interface by ferroelectric perovskites is particularly attractive. The spontaneous polarization present in these materials is very sensitive to electric fields and could be used to create a bound charge at the interface that could reinforce/deplete the 2DEG. Previous theoretical works have been focused on I-V/II-IV interfaces (NaNbO$_3$/SrTiO$_3$,[21,22] and KNbO$_3$/ATiO$_3$ interfaces, where $A =$ Sr, Ba, or Pb[22–24]). From the formal ionic charge point of view, I-V

ferroelectric perovskite oxides, such as $NaNbO_3$ and $KNbO_3$, are made of alternating positive $(B^{+5}O_2^{-2})^{+1}$ and negative $(A^{+1}O^{-2})^{-1}$ charged layers along the [001] direction (essentially as $LaAlO_3$, although now the AO layers of the perovskite ABO_3 structure are negative, while the BO_2 layers are positive). Therefore the layer-by-layer electrostatic of the previous I-V/II-IV interfaces is analogous to that in the $LaAlO_3/SrTiO_3$ interface. Density functional theory simulations on nonstoichiometric (i.e., with a noninteger number of unit cells of the layer-by-layer non neutral perovskite), symmetric superlattices indeed suggested the existence of a 2DEG in $KNbO_3/ATiO_3$ interfaces, switchable between two conducting states by the ferroelectric polarization orientation of the titanate layer.[23,24]

However, with the simulation boxes used in the previous works, only the *n*- or *p*-type interfaces are present. It can be proved (see Sec. 4 of Supplemental Material of Ref. 25) that, within this configuration, the local interface properties exactly reproduce those of the infinite isolated slab geometries, obviously beyond the critical thickness for the formation of the 2DEG. In other words, the calculations of Refs. 23 and 24 show the charge distribution and properties after the electronic reconstruction has taken place, but nothing is said about the magnitude of the critical thickness for the formation of the 2DEG.[26]

In this work, we carry out first-principles calculations of $BaTiO_3/KNbO_3$ interfaces where we explicitly avoid the issue of lack of stoichiometry in the simulation box. We have found that, due to the large lattice screening provided by the $KNbO_3$ layer, the critical thickness for the formation of the 2DEG is one order of magnitude larger than in $LaAlO_3/SrTiO_3$ interfaces. An unexpected result of our simulations is that an in-plane polarization develops on the $BaTiO_3$ side of a (TiO_2/KO) *p*-type $BaTiO_3/KNbO_3$ interface even when $BaTiO_3$ is subject to in-plane compressive strains. We explain this effect using basic electrostatic arguments.

The rest of the paper is organized as follows. After summarizing the basic theory behind the electronic reconstruction in Sec. II, we present the computational details used in our simulations in Sec. III. The first-principles results, together with the relevant comparisons to the model, can be found in Sec. IV.

II. BACKGROUND ON THE "POLAR DISCONTINUITY" MODEL

In order to establish the nomenclature and the basic theory that will be used later, we review the most important points of the "polar discontinuity" model. Although this model has been invoked since the discovery of the 2DEG at polar oxide interfaces,[9] only recently it has been rigorously rationalized with explanations firmly rooted on the modern theory of polarization (for a recent review, see Ref. 27 and references therein). This has been developed by Stengel and Vanderbilt in Ref. 10 for insulating interfaces, and later generalized by Stengel for the case of a nonzero surface density of "free" charge in Ref. 25, and to the case of surfaces in Ref. 28. The theory presented in these works is absolutely general, and we strongly point the interested reader to those milestone papers. Here, we particularize it to the conditions considered in this

work, and estimate the critical thickness for the formation of 2DEG in the case where any of the two materials forming the interface is ferroelectric.

The standard nomenclature used in the literature of polar oxide interfaces denote the materials that are nonneutral layer by layer (i.e., $LaAlO_3$) as *polar*, and the materials that are neutral layer by layer (i.e., $SrTiO_3$) as *nonpolar*. Rigorously, this notation does not apply here since the two materials that constitute our interfaces are ferroelectric and, therefore, might undergo polar phase transitions with the appearance of a nonvanishing spontaneous polarization. Nevertheless, for the sake of consistency with previous works, we will maintain the convention and refer to the ferroelectric nonneutral layer-by-layer material (i.e., $KNbO_3$) as the polar material and the ferroelectric neutral layer-by-layer material (i.e., $BaTiO_3$) as the nonpolar one.

During the development of the model we assume a *n*-type interface, simulated within an isolated slab geometry, with the nonpolar material at the left and the polar material (with a formal ionic charge of $\pm e$ alternating from layer to layer, where e is the magnitude of the electronic charge) at the right [see Fig. 1(a)]. The generalization for other configurations is straightforward, changing the appropriate signs when required.

Within the modern theory of polarization, we can compute the "formal" bulk polarization from the positions of the atomic nuclei and the center of localized Wannier functions. This decomposition of the charge (nuclear and electronic) into localized contributions allows for a simple classical interpretation of the bulk polarization in terms of a point charge model, and rescue the Clausius-Mossotti formulation.

In the perfectly ideal structure without rumpling, where an atomically sharp junction in the absence of defects is supposed, all the atoms at a given layer lie at the same plane [see Fig. 1(a)]. Then, we can always choose unit cells that tile the crystal under appropriate primitive translations, and that leave the leftover interface region charge neutral.[10] (It is important to note that, for the moment, we are assuming that the thickness of the polar layer is below the critical thickness for the formation of the 2DEG.) Then, the magnitude of the dipole of an individual (AO)-(BO_2) unit in this material is $d = ea/2$, where a is the out-of-plane lattice constant. The sign of the dipole is always directed from the negative to the positive layer, so in the considered configuration the sign is negative [see Fig. 1(a)]. This dipole corresponds to a "built-in formal" polarization (calculated for the previous choice of unit cell for the primitive basis of atoms and Wannier functions) of

$$P^0_{\text{polar}} = \frac{d}{\Omega} = -\frac{ea}{2aS} = -\frac{e}{2S}, \quad (1)$$

where Ω is the volume of the unit cell of the polar material and S is the cell surface. Analogously, since the layers are formally charged neutral in the nonpolar material, $P^0_{\text{nonpolar}} = 0$.

Now, we can wonder what would happen if the materials that constitute the interface are ferroelectric, with a nonvanishing ferroelectric contribution to the polarization P^S (this might be also the case when a compressive epitaxial strain is applied to the $SrTiO_3/LaAlO_3$ interface[29]). In this situation, the ferroelectric polarization must be added to the "built-in" polarization of the polar layer.[28]
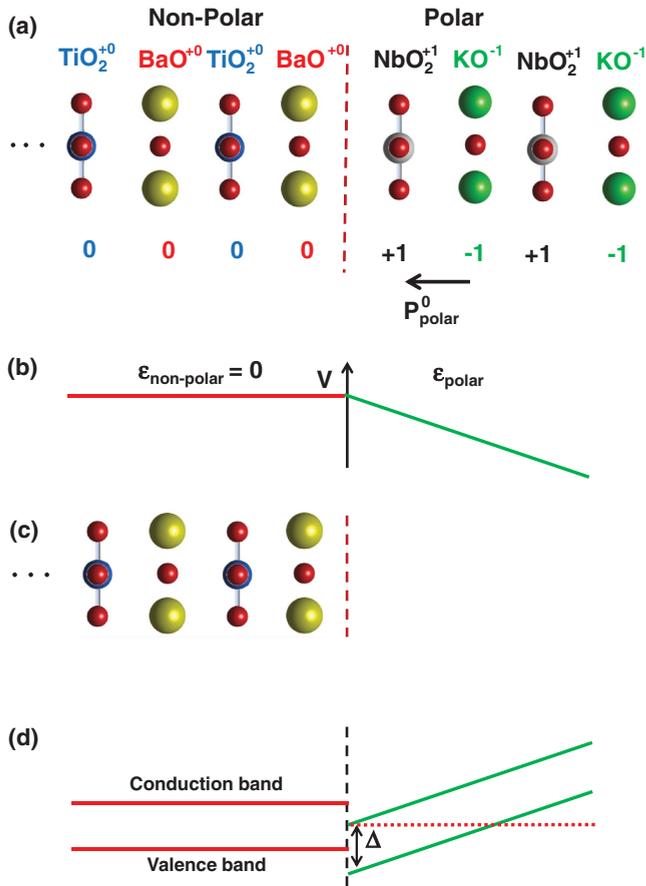
FIG. 1. (Color online) (a) Schematic representation of a pristine polar interface in an isolated slab geometry. Atoms are represented by balls: O (small size, red), Ba (large size, yellow), Ti (medium size, blue), K (large size, green), and Nb (medium size, gray), with the corresponding atomic layer printed on top. The dots at the left of the BaTiO$_3$ indicates that we assume a thick layer. At the other side, a free KO-terminated surface of the polar KNbO$_3$ is assumed. Numbers below each layer indicate the formal ionic charge. The interface is marked with a red dashed line. Our choice for the unit cells that tile the entire crystal are represented by black dashed boxes. a stands for the out-of-plane lattice constant of the polar material unit cell. (b) Electrostatic potential of the polar interface in the isolated slab geometry. Within our electrostatic boundary conditions, the macroscopic electric field in BaTiO$_3$ is forced to be zero. Note that the field within the nonneutral layers points away from the interface. (c) Induced polarizations ΔP due to the macroscopic electric fields. (d) Schematic representation of the energy bands of the polar interface.

The difference in the polarization at the interface between the two materials produces a surface density of bound charge,

$$\sigma_{\text{bound}} = P_{\text{nonpolar}} - P_{\text{polar}}. \tag{2}$$

Classical electromagnetic theory (Gauss's theorem) teaches us that this sheet of interfacial charge gives rise to a change in the macroscopic electric field in the two materials of

$$\mathcal{E}_{\text{polar}} - \mathcal{E}_{\text{nonpolar}} = \frac{\sigma_{\text{bound}}}{\epsilon_0}, \tag{3}$$

where ϵ_0 is the dielectric permittivity of vacuum [see Fig. 1(b)]. The exact magnitude of the fields depends on the electrostatic

boundary conditions, extremely linked with the geometry of the simulation boxes used in the computations (see Supplemental Material of Ref. 25 for a complete review).

The field might induce strong structural changes in the materials and polarizes the electronic Wannier functions. Both facts translate into the development of a field-induced polarization ΔP [see Fig. 1(c)] that tends to screen the discontinuity of the total polarization P,

$$P = P^0 + P^S + \Delta P \tag{4}$$

and, consequently, of the macroscopic electric field. At the end, a self-consistent solution of Eqs. (2)–(4) is achieved where the polarizations in the two materials are in equilibrium with the corresponding macroscopic electric fields, and the total energy of the system is minimized.

For a sufficiently thin polar layer thickness, before the electronic reconstruction takes place, the absence of free charge at the interface requires the normal component of the electric displacement field D to be preserved,

$$D_{\text{nonpolar}} = D_{\text{polar}} \equiv D. \tag{5}$$

The finite electric displacement is an input parameter of the model. In a first-principles simulation, its value can be set by hand using the virtual crystal approximation to introduce external fractional charges in the surface atoms layers, while constraining the macroscopic electric field to be strictly zero in the vacuum region.[25] Other authors fix the atomic positions on the surface unit cell to some specific values.[29]

From the definition of the electric displacement field,

$$
\begin{aligned}
D_{\text{polar}} &= \epsilon_0 \mathcal{E}_{\text{polar}} + P_{\text{polar}} \\
&= \epsilon_0 \mathcal{E}_{\text{polar}} + P^0_{\text{polar}} + P^S_{\text{polar}} + \Delta P_{\text{polar}},
\end{aligned} \tag{6}
$$

and assuming that the polar material behaves as a linear dielectric of susceptibility χ_{polar} around the spontaneous polarization structure, then

$$\Delta P_{\text{polar}} = \epsilon_0 \chi_{\text{polar}} \mathcal{E}_{\text{polar}}, \tag{7}$$

and Eq. (6) transforms into

$$D_{\text{polar}} = \epsilon_0 \epsilon_{\text{polar}} \mathcal{E}_{\text{polar}} + P^S_{\text{polar}} + P^0_{\text{polar}}, \tag{8}$$

where $\epsilon_{\text{polar}} = 1 + \chi_{\text{polar}}$ is the dielectric constant of the polar material. From Eqs. (5) and (8),

$$\mathcal{E}_{\text{polar}} = \frac{D - \left(P^0_{\text{polar}} + P^S_{\text{polar}}\right)}{\epsilon_0 \epsilon_{\text{polar}}}. \tag{9}$$

This electric field tilts the electronic bands of the polar layer [see Fig. 1(d)]. At a given critical thickness t_c, the top of the valence band of the polar material reaches the level of the bottom of the conduction bands.[30] Beyond t_c, a Zener breakdown takes place, with the concomitant transfer of charge from the surface of the polar material to the interface. The magnitude of t_c can be easily computed from Eq. (9) as

$$t_c = \frac{\Delta}{e|\mathcal{E}_{\text{polar}}|} = \frac{\epsilon_0 \epsilon_{\text{polar}} \Delta}{e\left|D - \left(P^0_{\text{polar}} + P^S_{\text{polar}}\right)\right|}, \tag{10}$$

where Δ is the interfacial potential step. Δ will depend on the type of band alignment and on the particular interface (p or n). Here, according to the band alignment of Fig. 1(d), for the n interface is given by[31]

$$\Delta = E^{\text{polar}}_{\text{gap}}, \tag{11}$$

where E_{gap}^{polar} is the band gap of the polar material. Note that the band alignment in our interfaces, where the band gaps of $BaTiO_3$ and $KNbO_3$ are very similar, is of type II, different from that in the prototypical $LaAlO_3/SrTiO_3$ case (type I). For schematic views of the types of interfaces according to the band offset see Fig. 1(b) of Ref. 32 for a type I interface and Fig. 1(a) of the same work for a type II interface.

The first conclusion that can be drawn from Eq. (10) is that the polarizability of the polar layer is essential to determine the critical thickness for the formation of the 2DEG (it is directly proportional to ϵ_{polar}). The role played by the polar distortions to avoid the polar catastrophe in $LaAlO_3/SrTiO_3$ interfaces has been confirmed by first-principles simulations.[33] The importance of the extra screening due to lattice relaxations has also been discussed in the strongly related $LaTiO_3/SrTiO_3$ interfaces.[34–36] Indeed, the success of explaining the critical thickness for the formation of the 2DEG,[17,20,26] together with the electrostrictive effect on the polar $LaAlO_3$ films,[37] is one of the most important achievements of the polar discontinuity model.

The second conclusion is related with the relationship between D and the ferroelectric polarization in the nonpolar layer. In many works, the simulations try to reproduce the behavior of a thin polar layer on top of a thick nonpolar substrate. In such cases, the macroscopic field in the nonpolar materials is forced to be zero, either by symmetry or by using a dipole correction in vacuum. As a consequence, $D = P_{nonpolar}$. If the ferroelectric contribution to the polarization in the nonpolar layer points in the same direction as the "built-in" polarization in the polar one, then it contributes to the increase of the critical thickness. This has been proven in Ref. 29 for the case of a $SrTiO_3/LaAlO_3$ interface subject to epitaxial strain [Eq. (10) is equivalent to Eq. (4) in Ref. 29 taking into account that, in this particular system, $P_{polar}^S = P_{LaAlO_3}^S = 0$ and $D = P_{SrTiO_3}^S$].

Finally, the third conclusion is that there is also a strong influence of an eventual spontaneous polarization of the polar material in the value of t_c. In particular, if P_{polar}^S is close in magnitude to P_{polar}^0 and points in the opposite direction, so the "built-in" polarization can be almost compensated by the ferroelectric contribution to the polarization, a large cancellation of the term in parentheses in the denominator of Eq. (10) is produced, with the concomitant increase in the critical thickness. In a previous work, Murray and Vanderbilt[38] have estimated how in $SrTiO_3/KNbO_3$ *superlattices* the system would not become metallic until the number of layers of $KNbO_3$ is larger than 32.

To further validate Eq. (10) in an *isolated slab* geometry, we have carried out simulations on $BaTiO_3/KNbO_3$ interfaces. The motivation for this choice is fourfold. (i) Under appropriate compressive in-plane strains, $KNbO_3$ is a ferroelectric polar material, with the spontaneous polarization pointing along the [001] direction, and with a "built-in" polarization of $P_{polar}^0 = P_{KNbO_3}^0 = e/2S \approx 53$ $\mu C/cm^2$ (a value computed at the theoretical in-plane lattice constant of a hypothetical $SrTiO_3$ substrate, $a_\parallel = 3.874$ Å). (ii) Under this mechanical boundary condition, both $KNbO_3$ and $BaTiO_3$ can be stabilized with the same tetragonal $P4mm$ symmetry. (iii) The theoretical spontaneous polarization of our tetragonal

$KNbO_3$ in bulk is $P_{polar}^S = P_{KNbO_3}^S = 48$ $\mu C/cm^2$, close to the built-in polarization. (iv) We can also test to which extent the ferroelectric contribution to the polarization in the $BaTiO_3$ layer is dominated by the imposed value of the displacement field in the simulations. First-principles results and comparison with the previous model will be presented in Sec. IV.

III. COMPUTATIONAL DETAILS

We have carried out density functional first-principles simulations based on a numerical atomic orbital method as implemented in the SIESTA code.[39] All the calculations have been carried out within the local density approximation (LDA), using the Perdew and Zunger[40] parametrization of the Ceperley and Alder functional[41] to simulate the electronic exchange and correlation. This choice avoids the systematic overestimation of the ferroelectric character[42] of perovskite oxides found in other commonly used functionals[43] based on the generalized gradient approximation. This is an important point in this study, since the dielectric properties of the oxides at the bulk level might determine the behavior of the interfaces, in particular, a tendency for "overscreening" of the 2DEG when the ferroelectric properties are favored.[25]

Core electrons were replaced by *ab initio* norm conserving pseudopotentials, generated using the Troullier-Martins scheme[44] in the Kleinman-Bylander fully nonlocal separable representation.[45] Due to the large overlap between the semicore and valence states, the semicore $3s$ and $3p$ electrons of Ti, $3s$ and $3p$ electrons of K, $4s$ and $4p$ electrons of Nb, and $5s$ and $5p$ electrons of Ba were considered as valence electrons and explicitly included in the simulations. K, Ti, Nb, and Ba pseudopotentials were generated scalar relativistically. The reference configuration and cutoff radii for each angular momentum shell for the pseudopotentials used in this work can be found in Ref. 46 for Ba, Ti, and O, and in Table I for K and Nb.

The one-electron Kohn-Sham eigenstates were expanded in a basis of strictly localized numerical atomic orbitals.[47,48] We used a single-ζ basis set for the semicore states of K, Ti, Nb, and Ba and double-ζ plus polarization for the valence states of all the atoms. For K (Ba), an extra shell of $3d$ ($5d$) orbitals was added. All the parameters that define the shape and range of the basis functions were obtained by a variational optimization of the energy[49] in bulk cubic $BaTiO_3$ (for Ba, Ti, and O), and

TABLE I. Reference configuration and cutoff radii of the pseudopotential used in our study. Because of the inclusion of the semicore states in valence within the Troullier-Martin scheme, K and Nb pseudopotentials must be generated for ionic configurations (ionic charge of $+1$). However, these are more suitable than the neutral ones, given the oxidation numbers of these atoms in the perovskites. Units in Bohr.

Reference		K $3s^2, 3p^6, 3d^0, 4f^0$	Nb $4s^2, 4p^6, 4d^4, 4f^0$
Core radius	s	1.50	1.45
	p	1.35	1.50
	d	1.50	1.40
	f	2.00	2.00
Scalar relativistic		yes	yes

of the entalphy[50] (with a pressure P = 0.03 GPa) in bulk cubic $KNbO_3$ (for K and Nb, the basis set of O was frozen to that obtained in $BaTiO_3$).

The electronic density, Hartree, and exchange correlation potentials, as well as the corresponding matrix elements between the basis orbitals, were calculated in a uniform real space grid. An equivalent plane-wave cutoff of 1200 Ry was used to represent the charge density. For the Brillouin zone integrations, we use a Monkhorst-Pack sampling[51] equivalent to $12 \times 12 \times 12$ in a five atom perovskite unit cell.

To avoid the problem of artificially charging the interface with the use of nonstoichiometric superlattices with periodic boundary conditions, we follow the proposal of Lee and Demkov.[26] Within this approach, the calculations were performed on vacuum-terminated $(KNbO_3)_m/(BaTiO_3)_l/(KNbO_3)_m$ slabs, where the number of $KNbO_3$ cells, m, is always an integer number to guarantee the electrical neutrality of the interface. In particular, we have focused on two kinds of systems: symmetric slabs where both interfaces between $BaTiO_3$ and $KNbO_3$ are of the same kind (either p-type TiO_2/KO, or n-type BaO/NbO_2 interfaces) and asymmetric interfaces where one interface is TiO_2/KO and the other BaO/NbO_2. In both cases, we have relaxed structures containing a different number of $KNbO_3$ and $BaTiO_3$ unit cells, given by the subscripts m and l, respectively. Note that l is an integer number in the asymmetric interfaces and an half-integer in the symmetric ones. In the asymmetric interface, a dipole slab correction is used to guarantee that the electric field in vacuum vanishes.

The in-plane lattice constant was fixed to the theoretical one of an hypothetical $SrTiO_3$ substrate ($a_\parallel = 3.874$ Å). Under this constraint, both $BaTiO_3$ and $KNbO_3$ are under conditions of compressive epitaxial strains. This will be relevant for the discussion of Sec. IV B. We have not considered the influence of octahedral rotations over these interfaces as both $BaTiO_3$ and $KNbO_3$ are highly resistant to this kind of distortion, even when $BaTiO_3$ thin films are strained to match the $SrTiO_3$ lattice parameter,[52] or $KNbO_3$ films are grown under a higher 5% compressive in-plane strains.[53]

Starting from ideal reference structures, built by piling up the corresponding unit cells of bulk strained materials without rumpling, the atomic coordinates are relaxed until the maximum component of the force on any atom was smaller than 0.01 eV Å^{-1}. In the symmetric slabs, the minimization is performed in a two step process. First, mirror symmetry planes are imposed on the central layer of $BaTiO_3$ to avoid the development of a polarization in any direction. Then, symmetry is broken displacing coherently the cations by hand, and a second relaxation is carried out without any imposed symmetry. In the asymmetric slabs, the relaxations are carried out in a single step, since the symmetry is broken directly in the initial reference structure. To establish the notation, we will call the plane parallel to the interface the (x,y) plane, whereas the perpendicular direction will be referred to as the z axis.

IV. RESULTS

A. Out-of-plane lattice relaxations and screening

In order to characterize the atomic displacements induced by the relaxation, we define the "out-of-plane" rumpling
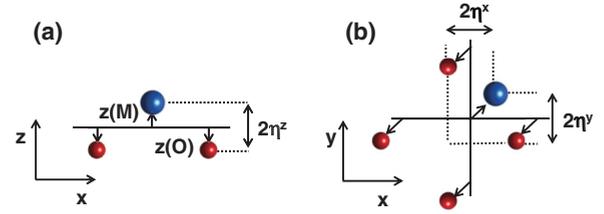

FIG. 2. (Color online) Schematic representation about the procedure to calculate (a) the out-of-plane rumpling η^z and (b) the in-plane rumplings η^x and η^y. Solid lines represent the position of the atoms in the ideal unrelaxed structure. After relaxation, the atoms move in the directions indicated by the arrows. Meaning of the balls as in Fig. 1.

parameter along z of layer i as $\eta_i^z = [z(M_i) - z(O_i)]/2$, where $z(M_i)$ and $z(O_i)$ are, respectively, the z coordinates of the cations and the oxygens at a given layer i [see Fig. 2(a)]. We also define the "in-plane" rumplings (η^x, η^y), in an equivalent way, as represented graphically in Fig. 2(b).

In all the studied systems, a large out-of-plane rumpling is observed within the $KNbO_3$ layers, with a magnitude that is essentially independent of their thickness and the kind of interface: symmetric p [see Fig. 3(a)], symmetric n [see Fig. 3(b)], or asymmetric [see Fig. 3(c)]. Two oxide layers away from the interface, the layer-by-layer rumpling converges to a rather uniform sawtooth pattern, with values slightly larger than those observed in bulk $KNbO_3$ under the same epitaxial conditions. This fact is consistent with $|P_{KNbO_3}^0| > |P_{KNbO_3}^S|$, with ΔP_{KNbO_3} tending to compensate for the difference in order to screen the polarization discontinuity at the interface. Only in the neighborhood of the free surface, a small deviation from this trend is obtained due to the larger relaxations on the surface atoms.

The dipole slab correction ensures that the displacement field in vacuum vanishes, $D = 0$. Due to the absence of surface external charges in the simulations, this value is preserved at the interfaces. This implies that a polarization in the $BaTiO_3$ layer induces a depolarizing field that is responsible for a large electrostatic energy. Therefore, under this electrical boundary conditions, no polarization is expected on $BaTiO_3$. Both facts are well reproduced in our simulations, where we observe that the out-of-plane polarization vanishes within the $BaTiO_3$ layer in all cases. This happens even when the mirror symmetries are lifted by hand (in the symmetric interfaces) or spontaneously (in the asymmetric slabs).

According to the model developed in Sec. II, the polarization in the polar layer tends to screen the discontinuity of the polarization at the interface and, therefore, its sign opposes that of the "formal" polarization. The lattice screening avoids the development of an electric field in the polar material that would result in the tilting of its bands and, for sufficiently large thicknesses, to a Zener breakdown and accumulation of charge at the interfaces. The lattice screening provided by $KNbO_3$ is much stronger than the one anticipated in $LaAlO_3$, where the structural distortion sustains the insulating behavior up to only five overlayers of $LaAlO_3$ on $SrTiO_3$.[33] As a consequence, in our simulations, all the computed structures are insulating. The reason behind this is that the $LaAlO_3$ is a wide band gap insulator with a low dielectric constant ($\epsilon_r = 25$) and no ferroelectric instability ($P_{LaAlO_3}^S = 0$). It costs
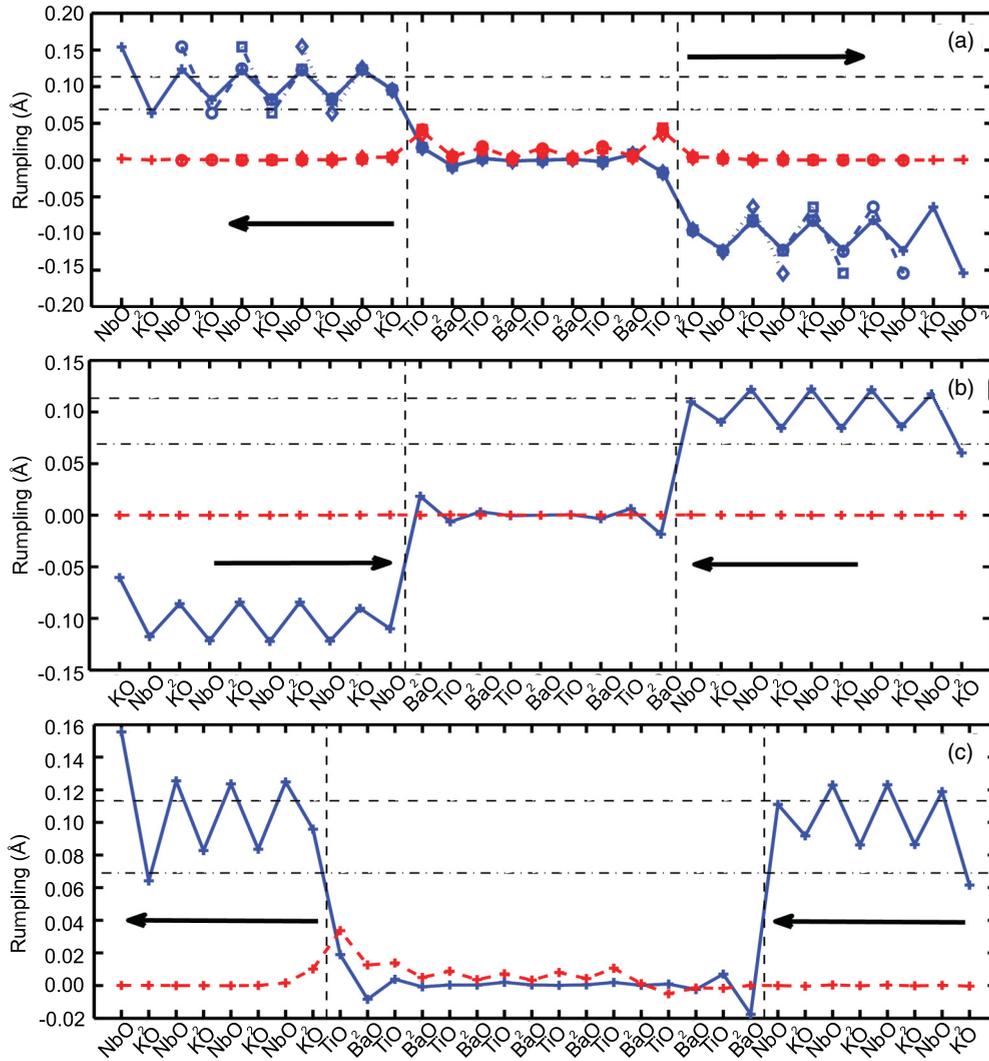
FIG. 3. (Color online) Out-of-plane (solid blue) and in-plane (long-dashed red) lattice polarization calculated for (a) symmetric-p [l fixed to 4.5 and $m = 2$ (diamonds), $m = 3$ (squares), $m = 4$ (circles), $m = 5$ (crosses)], (b) symmetric-n ($m = 5$, $l = 4.5$), and (c) asymmetric ($m = 4$, $l = 8$) BaTiO$_3$/KNbO$_3$ slabs. Short-dashed (dot-dashed) lines represent the rumplings of the NbO$_2$ (KO) layers in bulk KNbO$_3$ under the same epitaxial constraint. The arrows point along the direction of the "built-in" polarization. Vertical dashed lines indicate the position of the interfaces. The in-plane rumplings plotted here correspond to $\eta_{xy} = \sqrt{\eta_x^2 + \eta_y^2}$ defined in Fig. 2.

some energy to polarize it. On the contrary, KNbO$_3$ is a ferroelectric oxide that polarizes spontaneously, contributes to reduce the field [making smaller the numerator of Eq. (9)], and increase the critical thickness for the formation of the 2DEG [making larger the denominator of Eq. (10)]. The reduction of the internal field within KNbO$_3$ can be directly checked from the nanosmoothed[54,55] electrostatic potential in the slabs. Independently of the geometry, the magnitude of the field amounts to 0.024 V Å^{-1} [see red dashed lines in Fig. 4] to be compared with the roughly constant electric field of 0.24 V Å^{-1} (one order of magnitude larger) found in LaAlO$_3$/SrTiO$_3$ interfaces.[26,37] This is in very good agreement with the prediction of the electrostatic model developed in Sec. II: using a dielectric constant of bulk KNbO$_3$ around the ferroelectric structure under the same mechanical boundary condition of 25.0,[56] Eq. (9) yields a value of 0.023 V Å^{-1}.

Taking the experimental value of the indirect band gap of KNbO$_3$ in the cubic phase (3.3 eV)[57] and the valence band

offset between KNbO$_3$ and BaTiO$_3$ in the p-type interface as 0.24 eV (computed using the recipe given in Ref. 58 when the bands of one material are tilted), the estimated critical thickness to trigger the polar catastrophe under the condition of a vanishing electric displacement according to Eq. (10) is 133 and 143 Å for the p- and n-type interfaces (between 33 and 36 unit cells), respectively—one order of magnitude larger than in LaAlO$_3$/SrTiO$_3$. It is important to note that some authors have found experimentally that no more than 4 nm of coherently strained BaTiO$_3$ (around ten cells) can be grown on SrTiO$_3$.[59] This suggests that the formation of switchable 2DEGs by employing ferroelectric materials in interfaces might face additional difficulties in the structural stabilization of the interfaces, avoiding the formation of misfit dislocations.

B. In-plane polarization

Even though the ground state of bulk KNbO$_3$ and BaTiO$_3$ at zero temperature is rhombohedral, where the polarization

FIG. 4. (Color online) Macroscopically averaged internal electrostatic potential (black solid line) for (a) symmetric-p ($m = 5$, $l = 4.5$), (b) symmetric-n ($m = 5$, $l = 4.5$), and (c) asymmetric ($m = 4$, $l = 8$) BaTiO$_3$/KNbO$_3$ slabs. The red dashed lines indicates the region used to extract numerically the macroscopic field.

FIG. 5. (Color online) Schematic view of bulk unit cells of (a) BaTiO$_3$ and (b) KNbO$_3$, together with the ideal atomic structure at (c) p-type TiO$_2$/KO, and (d) n-type BaO/NbO$_2$ interfaces. Atoms are represented by balls following the same conventions as in Fig. 3. Numbers indicate the nominal charge of the different ions. Solid blue (dashed red) arrows represent an enhancement (depletion) of the in-plane electrostatic repulsion between ions. The schema shows how the replacement of ions favors the movement of the transition metal B-cation in TiO$_2$/KO interfaces and hinders it in the BaO/NbO$_2$ interfaces.

displays both in-plane (x, y) and out-of-plane (z) components, when a compressive in-plane strain is applied, the polarization in the (x, y) directions is strongly reduced or even suppressed.[52] In particular, when KNbO$_3$ or BaTiO$_3$ thin films are grown on top of a SrTiO$_3$ substrate, the in-plane polarization of these materials vanishes and the tetragonal c phase is stabilized.[60,61] However, contrary to current thought, in our calculations of the BaTiO$_3$/KNbO$_3$ interfaces, we can observe in Fig. 3 the appearance of a moderate in-plane polarization in these systems along the [110] direction. The layer-by-layer in-plane rumpling profile plotted in Fig. 3 reveals that the effect is highly localized at the p-type TiO$_2$/KO interface, quickly decaying upon moving into BaTiO$_3$, and it is completely absent at the n-type BaO/NbO$_2$ interfaces.

The origin of the hidden interfacial in-plane polarization can be easily understood with a simple electrostatic model based on formally charged ions. In Fig. 5, we compare the atomic structure of bulk BaTiO$_3$ [see Fig. 5(a)] and KNbO$_3$ [see Fig. 5(b)] with that present in the p-type TiO$_2$/KO [see Fig. 5(c)] and n-type BaO/NbO$_2$ [see Fig. 5(d)] interfaces. The cleavage of bulk BaTiO$_3$ and KNbO$_3$ to form the p-type TiO$_2$/KO interface is accompanied by a change in the local electrostatic potential felt by the Ti cations. At the interface, some of the Ba cations (nominal charge $+2$) in the first-neighbor atomic layer are replaced by K cations (nominal charge $+1$). This implies that at that interface the in-plane Ti cation movement is less constrained than in bulk, due to the reduced repulsions with K ions with respect to Ba ones. Analogously, in the n-type interface, the electrostatic potential felt by the Nb atoms is also altered. In this case, the K^{+1} cations are replaced by Ba^{+2} ions, leading to an enhanced repulsion that hinders the appearance of any in-plane polarization. As this effect is directly related to the nominal charges of the ions in both interfacial materials, we would expect it to be present in other similar systems and could be used to induce in-plane polarizations in other ferroelectric nanostructures.

To further characterize the development of the in-plane polarization, we take the relaxed coordinates of the asymmetric slab with $m = 5$ and $l = 8$ and remove by hand the in-plane displacements. We use this new structure as a reference configuration. Then, we compute the in-plane distortions required to go from the reference configuration to the relaxed structure and decompose into their x and y components. Finally, given fractions of these distortions are frozen in on top of the reference structure. The energy surface obtained for different fractions of the in-plane rumplings is represented in Fig. 6. From this energy landscape, we can extract (i) the stabilization energy (the energy difference between the polar state and the reference one), that amounts to 43.5 meV per slab, and (ii) the energy barriers that prevents the system to rotate the in-plane polarization from [110] direction to any of the other symmetry-equivalent positions, passing through the transition state at [100] positions. This is only 16 meV, slightly larger than those found in artificial Ruddlesden-Popper-type superlattices.[62] To gauge the magnitude of these barriers, we compare them with the rotation zero-point-energy (ZPE) in
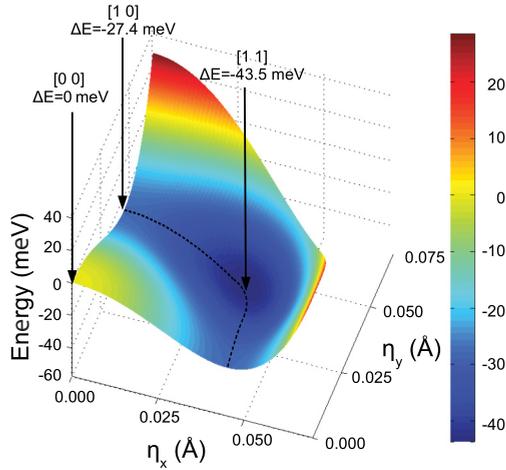
FIG. 6. (Color online) Two-dimensional energy surface as a function of the in-plane distortions of the $BaTiO_3$ atoms, as indicated in the main text. The dashed line follows the minimum of the valley. Units in milli-electron-volts.

this slab. This value is obtained through the nuclear motion Hamiltonian

$$\hat{H} = -\frac{\hbar^2}{2M^*}\left(\frac{\partial^2}{\partial \eta_x^2} + \frac{\partial^2}{\partial \eta_y^2}\right) + V(\eta_x, \eta_y), \quad (12)$$

where $V(\eta_x, \eta_y)$ is the energy represented in Fig. 6 and M^* can be shown to be

$$\frac{1}{M^*} = \sum_i \frac{c_i^2}{M_i}, \quad (13)$$

by writing the kinetic energy operator expressed in terms of atomic coordinates and masses (M_i) using the linear transformation relating the effective modes η_x and η_y with the atomic displacements through the coefficients c_i. In Eq. (12), $\eta_\alpha = \sum_i c_i (R_{i\alpha}^{(relax)} - R_{i\alpha}^{(0)})$, where $\alpha = x, y$ and $R_{i\alpha}^{(relax)}$ and $R_{i\alpha}^{(0)}$ are the α coordinates of the fully relaxed system when the in-plane distortion is taken into account and the tetragonal heterostructure, respectively. To solve the Schrödinger equation associated to Eq. (12) and find the vibrational levels associated to Fig. 6, we follow the recipe given in Ref. 63. Then, we compute the ZPE by comparing the position of the first level to the minimum of the energy surface. The resulting value for the ZPE, 13.6 meV, is much smaller than the global stabilization energy but comparable to the height of the rotational barrier, indicating that quantum fluctuations will be important in these nanostructures. These fluctuations prevent the observation of any in-plane spontaneous polarization, since the system will be delocalized over the four equivalent minima in [110] directions in a similar way to what happens in a dynamic Jahn-Teller problem.63

This case can be compared with what happens in an incipient ferroelectric. In the latter case, quantum fluctuations make the ZPE larger than the double well stabilization energy making the maximum of the probability density associated to the distortion (and the polarization) to be localized at the centrosymmetric state (origin in Fig. 6). On the other hand, in the present case, the maximum of the probability density corresponds with a nonzero polarization region around the origin (see dashed line in Fig. 6) but directional averaging results in a null net polarization. However, the coherent dynamics between the wells could be disrupted by small electric fields along the plane, which would induce large changes in the directionality of the in-plane polarization. The signature of such potential energy surface for polarization rotation would be a high dielectric constant.62

V. CONCLUSIONS

In summary, using accurate first-principles simulations we have studied the influence of the ferroelectric polarization of the polar layer in the formation of 2DEG at $BaTiO_3$/$KNbO_3$ interfaces. The most important conclusions that can be drawn are the following: (i) the spontaneous polarization of the polar $KNbO_3$ layer cancels out almost exactly the "built-in" polarization discontinuity at the interface; (ii) as a consequence of this compensation, the critical thickness for the formation of the 2DEG is estimated to be between 33 and 36 unit cells of $KNbO_3$, one order of magnitude larger than in $SrTiO_3$/$LaAlO_3$ interfaces; (iii) this behavior can be easily explained in terms of a simple model based on the modern theory of polarization and basic electrostatics; and (iv) surprisingly, $BaTiO_3$ displays an in-plane component of the polarization at the *p*-type TiO_2/KO interface, even when $BaTiO_3$ is under in-plane compressive strains. However, we do not expect this in-plane polarization to be experimentally observable as the barriers for its rotation are very small and quantum fluctuations will prevent it from being localized in a particular direction. This situation could be easily modified by the application of small electric fields that will break the symmetry and reveal the hidden polarization.

[1] A. Ohtomo and H. Y. Hwang, Nature (London), **427**, 423 (2004).

[2] J. Mannhart, D. H. A. Blank, H. Y. Hwang, A. J. Millis, and J.-M. Triscone, MRS Bull. **33**, 1027 (2008).

[3] J. Mannhart and D. G. Schlom, Science **327**, 1607 (2010).

[4] A. Brinkman, M. Huijben, M. van Zalk, J. Huijben, U. Zeitler, J. C. Maan, W. G. van der Wiel, G. Rijnders, D. H. A. Blank, and H. Hilgenkamp, Nat. Mater. **6**, 493 (2007).

[5]N. Reyren, S. Thiel, A. D. Caviglia, L. F. Kourkoutis, G. Hammerl, C. Richter, C. W. Schneider, T. Kopp, A. S. Rüetschi, D. Jaccard, M. Gabay, D. A. Muller, J. M. Triscone, and J. Mannhart, Science **317**, 1196 (2007).

[6]L. Li, C. Richter, S. Paetel, J. Mannhart, and R. C. Ashoori, Science **332**, 825 (2011).

[7]H. J. Gardner, A. Kumar, L. Yu, P. Xiong, M. P. Warusawithana, L. Wang, O. Vafek, and D. G. Schlom, Nat. Phys. **7**, 895 (2011).

[8]C. Cen, S. Thiel, J. Mannhart, and J. Levy, Science **323**, 1026 (2009).

[9]N. Nakagawa, H. Y. Hwang, and D. Muller, Nat. Mater. **5**, 204 (2006).

[10]M. Stengel and D. Vanderbilt, Phys. Rev. B **80**, 241103(R) (2009).

[11]P. R. Willmott, S. A. Pauli, R. Herger, C. M. Schlepütz, D. Martoccia, B. D. Patterson, B. Delley, R. Clarke, D. Kumah, C. Cionca, and Y. Yacoby, Phys. Rev. Lett. **99**, 155502 (2007).

[12]G. Herranz, M. Basletić, M. Bibes, C. Carrétéro, E. Tafra, E. Jacquet, K. Bouzehouane, C. Deranlot, A. Hamzić, J.-M. Broto, A. Barthélémy, and A. Fert, Phys. Rev. Lett. **98**, 216803 (2007).

[13]A. Kalabukhov, R. Gunnarsson, J. Borjesson, E. Olsson, T. Claeson, and D. Winkler, Phys. Rev. B **75**, 121404(R) (2007).

[14]N. C. Bristowe, P. B. Littlewood, and E. Artacho, Phys. Rev. B **83**, 205405 (2011).

[15]C. Cen, S. Thiel, G. Hammerl, C. W. Schneider, K. E. Andersen, C. S. Hellberg, J. Mannhart, and J. Levy, Nat. Mater. **7**, 298 (2008).

[16]W.-J. Soon, E. Cho, J. Lee, and S. Han, J. Phys.: Condens. Matter **22**, 315501 (2010).

[17]S. Thiel, G. Hammerl, A. Schmehl, C. W. Schneider, and J. Mannhart, Science **313**, 1942 (2006).

[18]Y. Hotta, T. Susaki, and H. Y. Hwang, Phys. Rev. Lett. **99**, 236805 (2007).

[19]M. Huijben, G. Rijnders, D. H. A. Blank, S. Bals, S. V. Aert, J. Verbeeck, G. V. Tendeloo, A. Brinkman, and H. Hilgenkamp, Nat. Mater. **5**, 204 (2006).

[20]H. Chen, A. M. Kolpak, and S. Ismail-Beigi, Phys. Rev. B **79**, 161402(R) (2009).

[21]R. Oja and R. M. Nieminen, Phys. Rev. B **80**, 205420 (2009).

[22]R. Oja, M. Tyunina, L. Yao, T. Pinomaa, T. Kocourek, A. Dejneka, O. Stupakov, M. Jelinek, V. Trepakov, S. van Dijken, and R. M. Nieminen, Phys. Rev. Lett. **109**, 127207 (2012).

[23]M. K. Niranjan, Y. Wang, S. S. Jaswal, and E. Y. Tsymbal, Phys. Rev. Lett. **103**, 016804 (2009).

[24]Y. Wang, M. K. Niranjan, S. S. Jaswal, and E. Y. Tsymbal, Phys. Rev. B **80**, 165130 (2009).

[25]M. Stengel, Phys. Rev. Lett. **106**, 136803 (2011).

[26]J. Lee and A. A. Demkov, Phys. Rev. B **78**, 193104 (2008).

[27]R. Resta and D. Vanderbilt, in *Physics of Ferroelectrics: a Modern Perspective*, Topics of Applied Physics (Springer, Berlin, 2007), pp. 31–68.

[28]M. Stengel, Phys. Rev. B **84**, 205432 (2011).

[29]C. W. Bark, D. A. Felker, Y. Wang, Y. Zhang, H. W. Jang, C. M. Folkman, J. W. Park, S. H. Baek, H. Zhou, D. D. Fong, Z. Q. Pan, E. Y. Tsymbal, M. S. Rzchowski, and C. B. Eom, PNAS **108**, 4720 (2011).

[30]M. L. Reinle-Schmitt, C. Cancellieri, D. Li, D. Fontaine, M. Medarde, E. Pomjakushina, C. W. Schneider, S. Gariglio, Ph. Ghosez, J.-M. Triscone, and P. R. Willmott, Nat. Commun. **3**, 932 (2012).

[31]For a p interface of type II, $\Delta = E_{\mathrm{gap}}^{\mathrm{polar}} - (E_{\mathrm{VBM}}^{\mathrm{nonpolar}} - E_{\mathrm{VBM}}^{\mathrm{polar}})$, where E_{VBM} is the valence band maximum of the corresponding layer right at the interface.

[32]J. Tersoff, Phys. Rev. B **30**, 4874 (1984).

[33]R. Pentcheva and W. E. Pickett, Phys. Rev. Lett. **102**, 107602 (2009).

[34]D. R. Hamann, D. A. Muller, and H. Y. Hwang, Phys. Rev. B **73**, 195403 (2006).

[35]S. Okamoto, A. J. Millis, and N. A. Spaldin, Phys. Rev. Lett. **97**, 056802 (2006).

[36]P. Larson, Z. S. Popovic, and S. Satpathy, Phys. Rev. B **77**, 245122 (2008).

[37]C. Cancellieri, D. Fontaine, S. Gariglio, N. Reyren, A. D. Caviglia, A. Féte, S. J. Leake, S. A. Pauli, P. R. Willmott, M. Stengel, Ph. Ghosez, and J.-M. Triscone, Phys. Rev. Lett. **107**, 056102 (2011).

[38]E. D. Murray and D. Vanderbilt, Phys. Rev. B **79**, 100102(R) (2009).

[39]J. M. Soler, E. Artacho, J. D. Gale, A. García, J. Junquera, P. Ordejón, and D. Sánchez-Portal, J. Phys.: Condens. Matter **14**, 2745 (2002).

[40]J. P. Perdew and A. Zunger, Phys. Rev. B **23**, 5048 (1981).

[41]D. M. Ceperley and B. J. Alder, Phys. Rev. Lett. **45**, 566 (1980).

[42]J. Junquera and Ph. Ghosez, J. Comput. Theor. Nanosci. **5**, 2071 (2008).

[43]J. P. Perdew, K. Burke, and M. Ernzerhof, Phys. Rev. Lett. **77**, 3865 (1996).

[44]N. Troullier and J. L. Martins, Phys. Rev. B **43**, 1993 (1991).

[45]L. Kleinman and D. M. Bylander, Phys. Rev. Lett. **48**, 1425 (1982).

[46]J. Junquera, M. Zimmer, P. Ordejón, and Ph. Ghosez, Phys. Rev. B **67**, 155327 (2003).

[47]O. F. Sankey and D. J. Niklewski, Phys. Rev. B **40**, 3979 (1989).

[48]E. Artacho, D. Sánchez-Portal, P. Ordejón, A. García, and J. M. Soler, Phys. Status Solidi B **215**, 809 (1999).

[49]J. Junquera, O. Paz, D. Sánchez-Portal, and E. Artacho, Phys. Rev. B **64**, 235111 (2001).

[50]E. Anglada, J. M. Soler, J. Junquera, and E. Artacho, Phys. Rev. B **66**, 205101 (2002).

[51]H. J. Monkhorst and J. D. Pack, Phys. Rev. B **13**, 5188 (1976).

[52]O. Diéguez, S. Tinte, A. Antons, C. Bungaro, J. B. Neaton, K. M. Rabe, and D. Vanderbilt, Phys. Rev. B **69**, 212101 (2004).

[53]G. Lee, Y.-H. Shin, and J. Y. Son, J. Am. Ceram. Soc. **95**, 2773 (2012).

[54]L. Colombo, R. Resta, and S. Baroni, Phys. Rev. B **44**, 5572 (1991).

[55]J. Junquera, M. H. Cohen, and K. M. Rabe, J. Phys.: Condens. Matter **19**, 213203 (2007).

[56]M. Stengel (private communication).

[57]E. Wiesendanger, Ferroelectrics **6**, 263 (1974).

[58]M. Stengel, D. Vanderbilt, and N. A. Spaldin, Phys. Rev. B **80**, 224110 (2009).

[59]H. P. Sun, W. Tian, X. Q. Pan, J. H. Haeni, and D. G. Schlom, Appl. Phys. Lett. **84**, 3298 (2004).

[60]Y. Yoneda, T. Okabe, K. Sakaue, H. Tekauchi, H. Kasatani, and K. Deguchi, J. Appl. Phys. **83**, 2458 (1998).

[61]Y. Yoneda, T. Okabe, K. Sakaue, and H. Tekauchi, Surf. Sci. **410**, 62 (1998).

[62]S. M. Nakhmanson and I. Naumov, Phys. Rev. Lett. **104**, 097601 (2010).

[63]P. García-Fernández, A. Trueba, M. T. Barriuso, J. A. Aramburu, and M. Moreno, Phys. Rev. Lett. **104**, 035901 (2010).